Supporting Information

Zn^{2+} Stabilized Pd Clusters with Enhanced Covalent Metal-Support Interaction via Forming Pd-Zn Bond to Promote Catalytic Thermal Stability

Kai-Qiang Jing,[a,b] Yu-Qing Fu,[a,b] Zhi-Qiao Wang,[a] Zhe-Ning Chen,[a]
Hong-Zi Tan,[a] Jing Sun,[a] Zhong-Ning Xu,*[a] and Guo-Cong Guo*[a]

[a] *State Key Laboratory of Structural Chemistry, Fujian Institute of Research on the Structure of Matter, Chinese Academy of Sciences, Fuzhou, Fujian 350002, P. R. China.*

[b] *University of Chinese Academy of Sciences, Beijing 100049, P. R. China.*

**E-mail: gcguo@fjirsm.ac.cn; znxu@fjirsm.ac.cn*

Experimental Procedures

Materials

The following materials and reagents were used as starting materials: Magnesium nitrate hexahydrate [$Mg(NO_3)_2 \cdot 6H_2O$, A.R., Sinopharm Chemical Reagent Co. (SCRC)], Aluminium nitrate nine hydrate [$Al(NO_3)_3 \cdot 9H_2O$, A.R., SCRC], Zinc nitrate hexahydrate [$Zn(NO_3)_2 \cdot 6H_2O$, A.R., SCRC], Hexamethylenetetramine [$C_6H_{12}N_4$], $Pd(acac)_2$ [AR; Kunming Institute of Precious Metals], Ethanol [EtOH, SCRC], deionized water.

Preparation of MgAl-LDH Support and Zn^{2+}-modified MgAl-LDH Support

The MgAl-LDH nanosheets with the ratio of Mg and Al (2:1) were synthesized by a facile hydrothermal process. 0.015 mol $Mg(NO_3)_2 \cdot 6H_2O$ and 0.0075 mol $Al(NO_3)_3 \cdot 9H_2O$ were added into 60 ml of deionized water. After stirring several minutes, 0.0195 mol of hexamethylenetetramine was put into the reacted system and the mixture was then transferred into a 100 mL Teflon-lined stainless steel autoclave. The autoclaves were put in an oven and hydrothermally treated at 140 °C for 24 h. After they were cooled to the room temperature, the white products were centrifuged and washed by ethanol and deionized water for many times. Finally, the prepared samples were dried at 60 °C in a vacuum oven.

Zn^{2+}-modified MgAl-LDH (denoted as ZnMgAl-LDH) were prepared by the same procedure as MgAl-LDH support except the addition of 0.0035 mol $Zn(NO_3)_2 \cdot 6H_2O$ on the first step over the preparation of MgAl-LDH Support.

The MgAl-LDH support with the ratios of Mg and Al (1:1 and 3:1) were prepared by the same procedure as the MgAl-LDH support with the ratio of Mg and Al (2:1) except the $Mg(NO_3)_2 \cdot 6H_2O$ was 0.0075 and 0.0225 mol, respectively.

Preparation of Pd/MgAl-LDH and Pd/ZnMgAl-LDH Catalysts via ALD technique.

The Pd/MgAl-LDH and Pd/ZnMgAl-LDH catalysts were fabricated via the atomic layer deposition technique (ALD). Pd ALD was carried out on a viscous flow reactor at 150 °C using palladium hexafluoroacetylacetate ($Pd(hfac)_2$, Sigma Aldrich, 99.9%) and formalin (Aldrich, 37% HCHO and 15% CH_3OH in aqueous solution). Ultrahigh purity N_2 (99.999%) was used as carrier gas at a flow rate of 200 $mL \cdot min^{-1}$. The $Pd(hfac)_2$ precursor container was heated to 65 °C to get a sufficient vapour pressure. The chamber was heated to 150 °C and the manifold was held at 110 °C to avoid precursor condensation. The timing sequence was 8, 20, 12 and 25 seconds for $Pd(hfac)_2$ exposure, N_2 purge, formalin exposure and N_2 purge, respectively. Before an ALD experiment, 400 mg samples were dispersed in a beaker with 10 mL ethanol using an ultrasonic. The above dispersion liquid was deposited on a new glass sheet surface and dried in air. After performing 30 Pd ALD cycles, the Pd/MgAl-LDH and Pd/ZnMgAl-LDH catalysts were calcined at 200 °C for 2 h in a nitrogen atmosphere.

Preparation of Pd/MgAl-LDH-Imp and Pd/ZnMgAl-LDH-Imp Catalysts.

The Pd/MgAl-LDH-Imp catalyst was prepared by a wet impregnation method: 0.0286 g of Pd(acac)$_2$ was dissolved in 25 mL of ultrapure water to form a yellow solution, and then 1.0 g of MgAl-LDH support was dispersed into the solution with vigorous magnetic stirring at room temperature for 10 h. The solid product was centrifuged and dried at 80 °C for 12 h under vacuum. The dried sample was calcined at 200 °C for 2 h in a 10% H_2/Ar atmosphere. The theoretical Pd loading of the catalyst is 1.0 wt %. The Pd/ZnMgAl-LDH-Imp catalyst was prepared by the same procedure as Pd/MgAl-LDH-Imp except the MgAl-LDH support was changed into ZnMgAl-LDH.

Preparation of MgAl-LDO and ZnMgAl-LDO Supports.

The MgAl-LDO support was prepared as follows: the MgAl-LDH support were placed in the quartz boat and heated in tube furnace under a gas flow of N_2 for 2 h at 400 °C. The heating of the thermal treatments was stepped at 2 $°C \cdot min^{-1}$. After they were cooled to the room temperature, the products were collected (denoted as MgAl-LDO).The ZnMgAl-LDO support was prepared by the same procedure as MgAl-LDO except the MgAl-LDH support was changed into ZnMgAl-LDH.

Preparation of Pd/MgAl-LDO-Imp and Pd/ZnMgAl-LDO-Imp Catalysts.

The Pd/MgAl-LDO-Imp catalyst and Pd/ZnMgAl-LDO-Imp catalyst were prepared by the same procedures as Pd/MgAl-LDH-Imp Pd/ZnMgAl-LDH-Imp except the MgAl-LDH support and ZnMgAl-LDH support were changed into MgAl-LDO and ZnMgAl-LDO supports.

Computational methods and models

Computational details and models: All density functional theory (DFT) calculations were performed through using the Vienna ab initio simulation package (VASP) and the projected augmented wave (PAW) method. The generalized gradient approximation (GGA) of the Perdew–Burke–Ernzerhof (PBE) exchange–correlation functional was employed. The kinetic energy cutoff plane–wave expansion was set to 400 eV. For geometric optimization, the total energy convergence was set to be smaller than 10^{-5} eV, and the force convergence was set to be lower than 0.01 eV/Å. Brillouin zone sampling was employed using a Monkhorst-Packing grid 3×3×1.

Firstly, the optimized lattice constants were a =5.265 Å，b = 9.114 Å，c =7.766 Å for MgAl-LDH, consistent with experimental and theoretical studies. Then, we built one MgAl-LDH support unit cell model. The support of MgAl-LDH and ZnMgAl-LDH could obtain metal-O$^-$ via deprotonation of hydroxyl groups followed by metal–oxygen coordination, achieving the supports with one H ion relaxed. Pd_{13} cluster was used as the model species of Pd(0) catalysts. Next, the Pd_{13} cluster was put into the space of MgAl-LDH. In the condition of Pd_{13}/MgAl-LDH, Pd_{13} cluster could bond to oxygen, further forming Pd_{13}-O-MgAl-LDH. In the condition of Pd_{13}/ZnMgAl-LDH, one Zn atom substitutes one Mg atom in the support of MgAl-LDH. When the Pd_{13} cluster is closed to ZnMgAl-LDH support, the structure of ZnMgAl-LDH has a slight change, forming Pd_{13}-Zn-O-MgAl-LDH.

The adsorption energy was defined as $E_{ads}= [E_{sp}+E_{pd}]-E_{pd/sp}$; where $E_{pd/sp}$ and E_{sp} is the total energy of the supports with and without adsorbate Pd_{13}, and E_{pd} was the energy of Pd_{13}.

In order to verify the exact configuration in experiments, the surface energies of two models were calculated (Table S4).

Characterization

XRD: The as-prepared samples were characterized by powder X-ray diffraction (XRD) on a glass wafer by a Rigaku MiniFlex 600 diffractometer with a Cu Kα X-ray source (λ =1.5406 Å) in the range of 5−85° (2θ).

UV−DRS and FT-IR: UV−visible diffuse reflectance spectra (UV−DRS) were measured on a PerkinElmer Lambda 950 spectrophotometer equipped with a diffuse reflectance accessory, and the spectra were recorded in the range of 200−800 nm using $BaSO_4$ as the reference sample. A Nicolet Nexus 670 Fourier transform infrared spectrometer was used to record the Fourier transform infrared (FT-IR) spectra of LDHs at a resolution of 4 cm^{-1}.

BET: The BET surface area and pore volume of the different samples were determined by N_2 adsorption−desorption at liquid nitrogen temperature (77 K), which was performed on a Micromeritics ASAP 2020.

TG: Thermogravimetric analysis (TGA) experiments were performed on a Mettler Toledo STAR SYSTEM in N_2 with the sample heated in an Al_2O_3 crucible at a heating rate of 10 °C/min.SEM: The morphologies of the samples were observed by scanning electron microscopy (SEM, JEOL JSM-6700F).

TEM, HAADF-STEM and HAADF-STEM EDS mapping: Transmission electron microscopy (TEM), high-resolution TEM (HRTEM), energy dispersive X-ray spectroscopy (EDS) analysis, high angle annular dark field scanning transmission electron microscopy (HAADF-STEM) and HAADF-STEM EDS mapping were performed on a Tecnai G2 F20 fieldemission transmission electron microscope operating at an acceleration voltage of 200 kV.

ICP: Inductively coupled plasma-optical emission spectroscopy (ICP-OES) data for the content of Pd was carried out on an Ultima-2 ICP emission spectrometer.

XPS: X-ray photoelectron spectroscopy (XPS) measurements were performed with a VG Escalab 250Xi spectrometer equipped with an Al anode (Al Kα = 1486.6 eV). The binding energies obtained in the XPS spectral analysis were corrected for specimen charging by referencing C 1s to 284.8 eV.

XAFS: XAFS measurements at Pd K-edge (24350 eV) were performed in fluorescence mode with solid probe at the Si (311) monochromator at BL14W1 beamline of the Shanghai Synchrotron Radiation Facility (SSRF), China. XAFS measurements at Zn K-edge (9659 eV) were performed in transmission mode with the Si (311) monochromator at BL14W1 beamline of the Shanghai Synchrotron Radiation Facility (SSRF), China.

***In situ* DR-FTIRS:** In situ diffuse reflectance Fourier transform infrared spectroscopy (DR-FTIRS) measurements were performed on a Nicolet 6700 diffuse reflectance infrared spectrometer equipped with a stainless steel in situ IR flow cell. A 45 mg portion of sample was placed into the cell, having been pretreated in N_2 flow for 20 min at 180 °C. After cooling to room temperature, a background spectrum was collected. Then, the sample was exposed to a flowing 5% CO/N_2 mixture (30 mL/min) for 30 min. Subsequently, the sample was purged with N_2 for 10 min to flush the CO in the gaseous mixture, and the spectrum was collected again.

In situ DR-FTIRS measurements of the reaction of CO and methyl nitrite (MN) to DMO were performed on a Nicolet 6700 diffuse reflectance infrared spectrometer equipped with a stainless steel in situ IR flow cell. A 45 mg portion of sample was placed into the cell, having been pretreated in N_2 flow for 20 min at 180 °C. After cooling to room temperature, a background spectrum was collected. Subsequently, the cell was heated to 130 °C. The CO and MN were introduced into the reactive system, and then, the FTIR spectra of the samples were collected.

CO pulse chemisorption and TPD: CO pulse chemisorption and temperature-programmed desorption (TPD) of CO_2 experiments were carried out using an Altamira AMI-300 instrument equipped with a thermal conductivity detector. The dispersion and surface area of Pd for catalysts were calculated from the amount of chemisorbed CO. In a typical CO_2-TPD experiment, about 100 mg of the samples were loaded in a quartz reactor and heated in He for 120 min at 200 °C, followed by treating with CO_2 in flow ($50\ mL{\cdot}min^{-1}$) for 60 min at 80 °C. Weakly adsorbed probe molecules were removed by flowing He for 60 min at 80 °C, and then the desorption process was carried out from 80 °C to 500 °C at 5 °C min^{-1} in the He flow.

Activity Evaluation

The activities of the catalysts for CO oxidative coupling to DMO were carried out in a fixed-bed quartz tubular reactor. The catalysts (200 mg) were placed in the center of the quartz tubular reactor. The reactant gases (28% CO, 18% CH_3ONO, 4% Ar as internal standard, and 50% N_2 as the balance gas) were passed through the reactor at a gas hourly space velocity (GHSV) of 3000 h^{-1}. The catalytic activity tests were performed under atmospheric pressure. The composition of the reactant gases and reaction products was monitored by an online Shimadzu GC-2014 gas chromatograph equipped with a thermal conductivity detector and a flame ionization detector.

The concentration ratio of CO and CH_3ONO in our reactant gases is 1.56:1, whereas the stoichiometry of CO and CH_3ONO in the reaction is 1:1. Therefore, CO is in excess, and the theoretical maximum value of CO conversion is 64.3%.

The conversion of CO, the selectivity to DMO, and the space-time yields (STY) of DMO were calculated using the following formulas:

Conversion of CO (%) = $([CO]_{in}/[Ar]_{in}-[CO]_{out}/[Ar]_{out})/([CO]_{in}/[Ar]_{in})\times 100\%$

Selectivity to DMO (%) = $(S_{DMO}\times R\text{-}F_{DMO})/(S_{DMO}\times R\text{-}F_{DMO}+S_{DMC}\times R\text{-}F_{DMC})\times 100\%$

STY of DMO ($g\cdot L^{-1}\cdot h^{-1}$) =conversion of CO × selectivity to DMO ×GHSV of CO×118.09 $g\cdot mol^{-1}$ /(2 ×22.4 $L\cdot mol^{-1}$)

where $[Ar]_{in}$ and $[Ar]_{out}$ are the concentrations of Ar at the inlet and outlet and $[CO]_{in}$ and $[CO]_{out}$ are the concentrations of CO at the inlet and outlet, respectively. S_{DMO} and S_{DMC} are the peak areas of dimethyl oxalate and dimethyl carbonate, $R\text{-}F_{DMO}$ and $R\text{-}F_{DMC}$ are the relative correction factors of dimethyl oxalate and dimethyl carbonate, respectively.

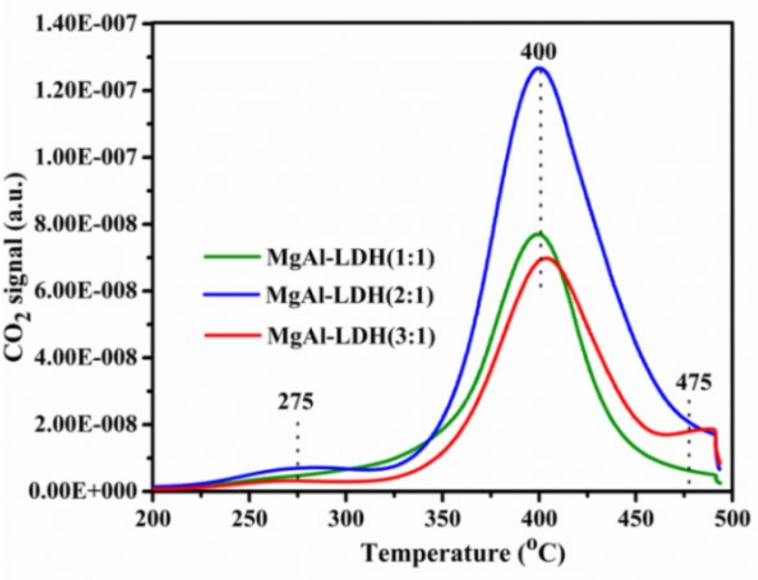

Fig. S1. CO_2-TPD curves of the MgAl-LDH supports with the different ratio of Mg and Al.

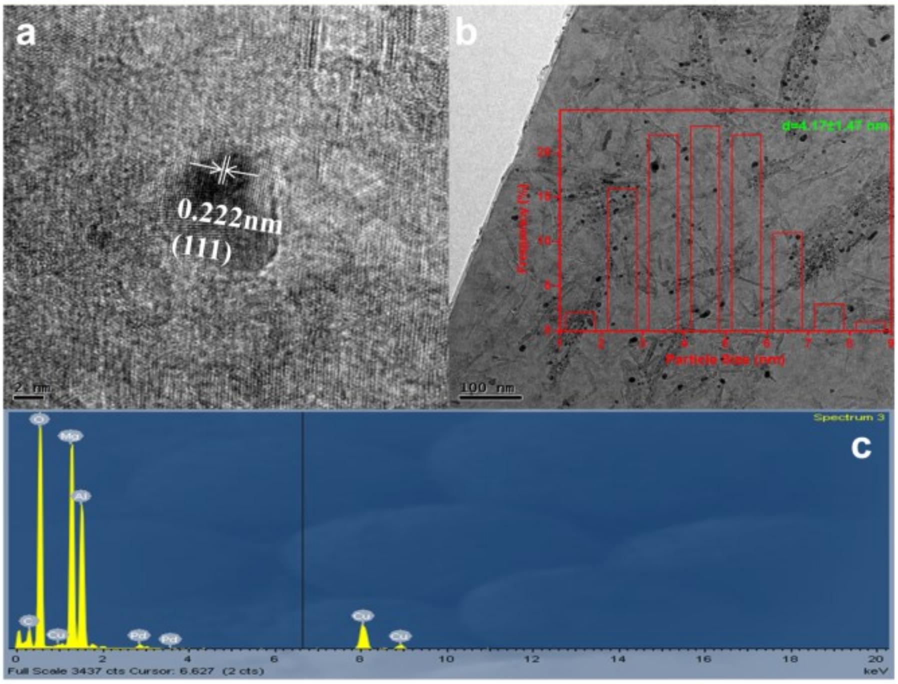

Fig. S2. Characterizations of the Pd/MgAl-LDH prepared by the method of impregnation. (a) HRTEM image. (b) TEM image and Size distribution of the Pd NPs. (c) EDS analysis.

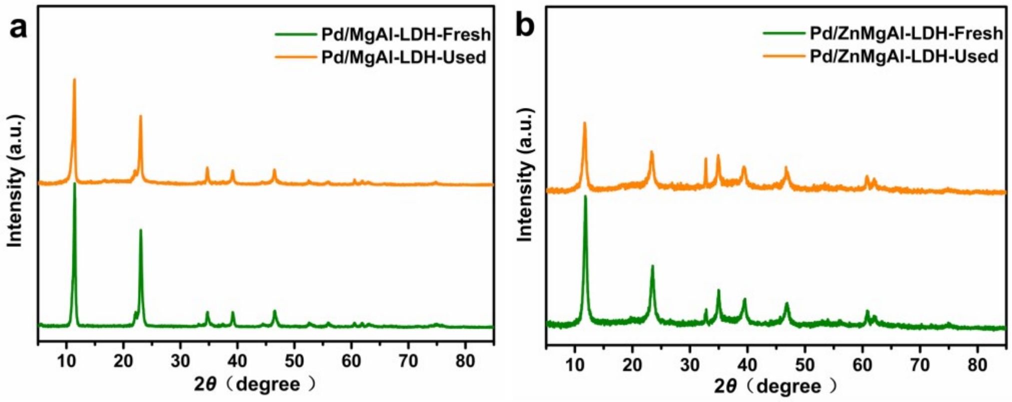

Fig. S3. (a) XRD patterns of the fresh and used Pd/MgAl-LDH (ALD) catalyst. (b) Fresh and used Pd/ZnMgAl-LDH (ALD) catalyst.

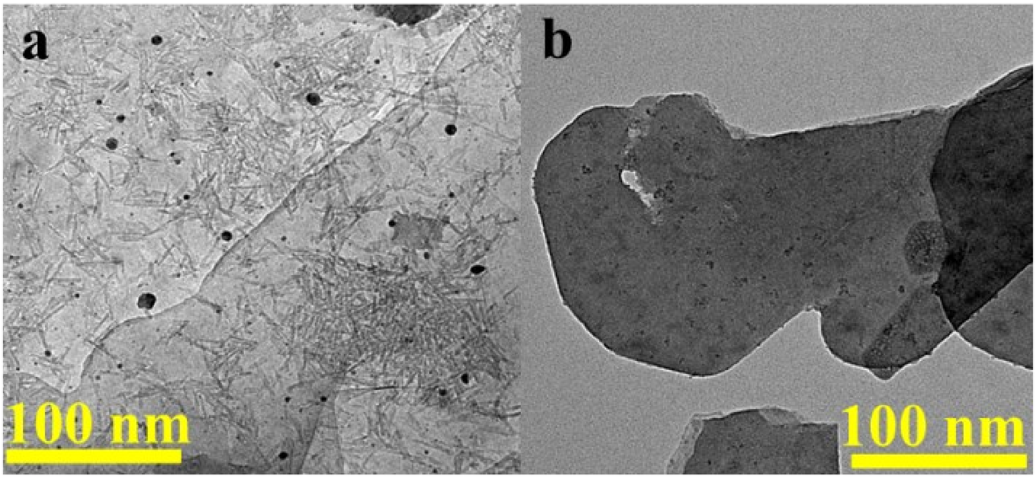

Fig. S4. The TEM images for the used Pd/MgAl-LDH (a) and Pd/ZnMgAl-LDH (b).

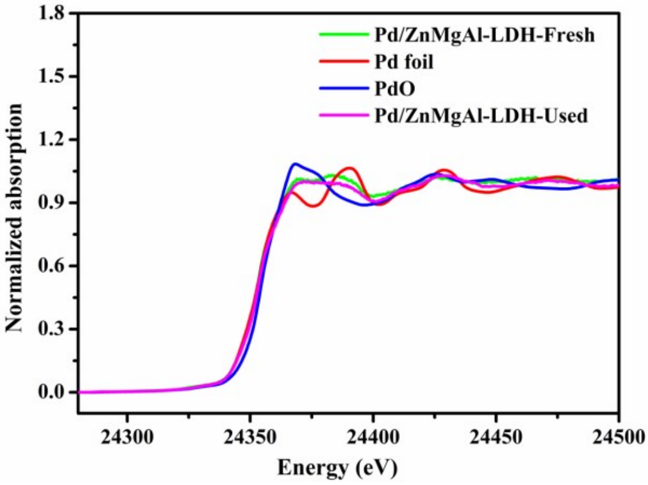

Fig. S5. Pd K-edge XANES spectra of fresh and used Pd/ZnMgAl-LDH (ALD), Pd foil and PdO.

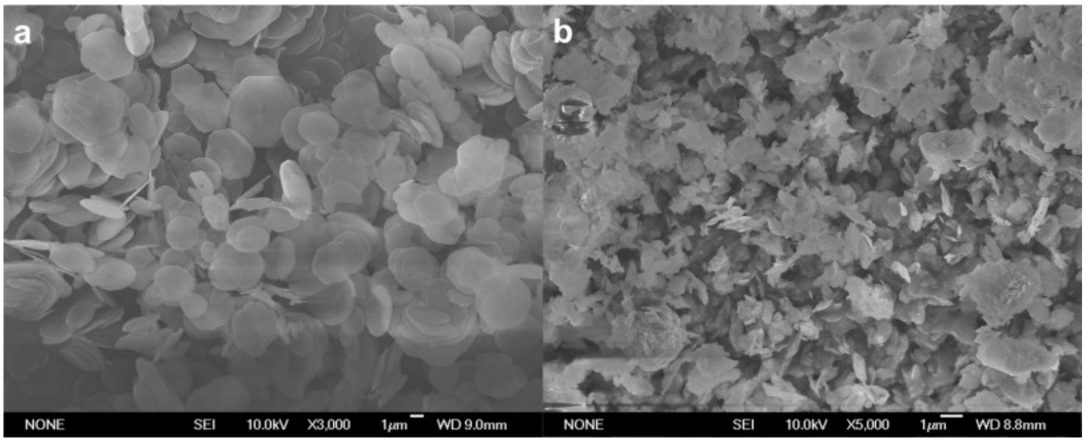

Fig. S6. SEM images of (a) MgAl-LDH. (b) ZnMgAl-LDH supports.

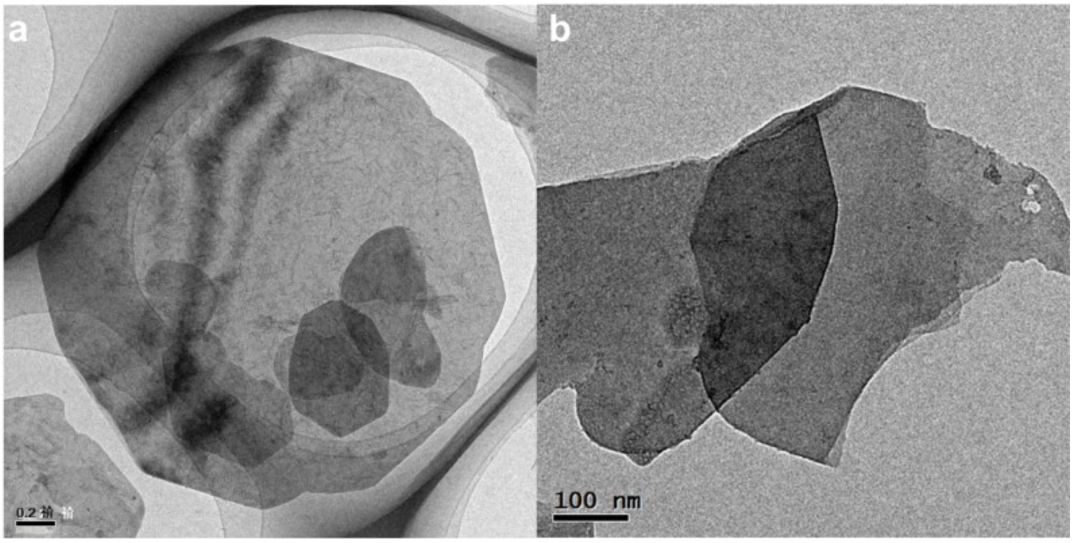

Fig. S7. TEM images of (a) MgAl-LDH. (b) ZnMgAl-LDH supports.

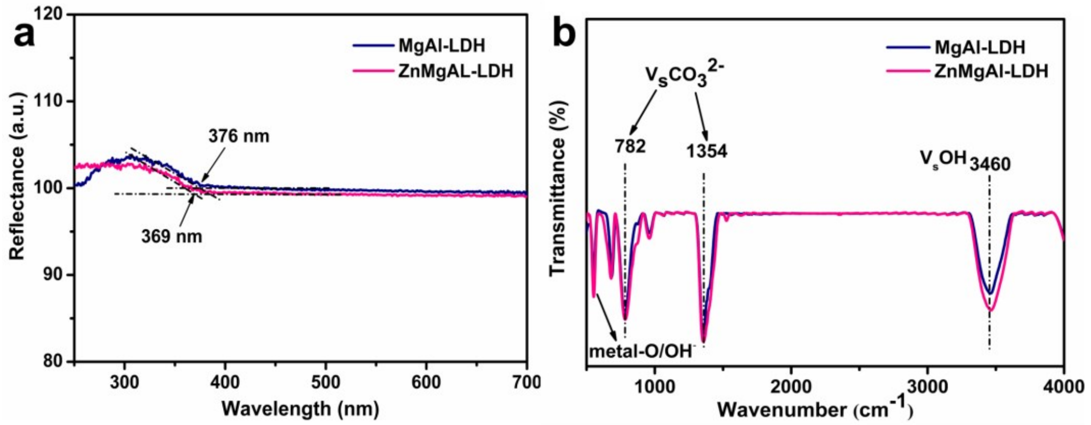

Fig. S8. (a) UV−DRS profiles of MgAl-LDH and ZnMgAl-LDH supports. (b) FT-IR spectra MgAl-LDH and ZnMgAl-LDH supports.

The FT-IR spectra of the prepared samples are shown in Fig. S8b. A strong broad absorption band at 3460 cm^{-1} can be observed for both samples, attributing to stretching vibration of hydroxyl groups and interlayer water molecules[3]. The strong peaks at 1354 cm^{-1} and 782 cm^{-1} can be assigned to the symmetric stretching vibrations and out-of-plane deformation of the interlayer carbonate ions, respectively. Moreover, the other peaks below 800 cm^{-1} are the vibrations of metal-O bonds and metal-OH bonds in the LDH lattice[1].

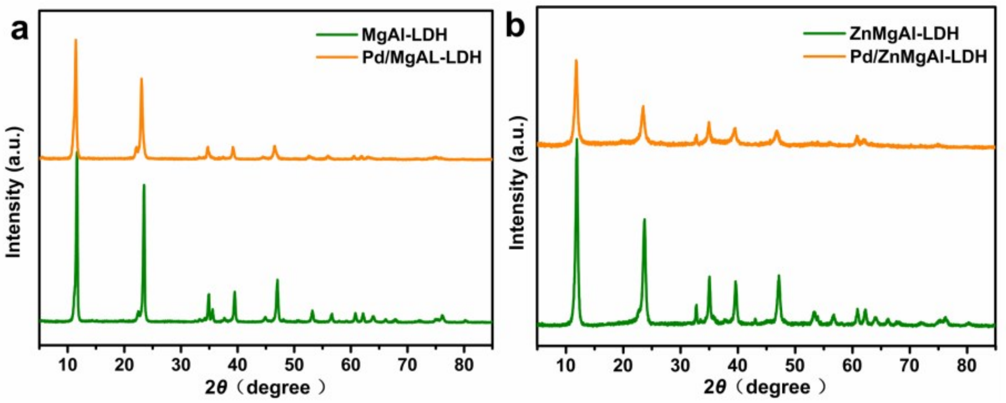

Fig. S9. XRD patterns of the prepared samples. (a) MgAl-LDH and Pd/MgAl-LDH prepared by ALD. (b) ZnMgAl-LDH and Pd/ZnMgAl-LDH prepared by ALD.

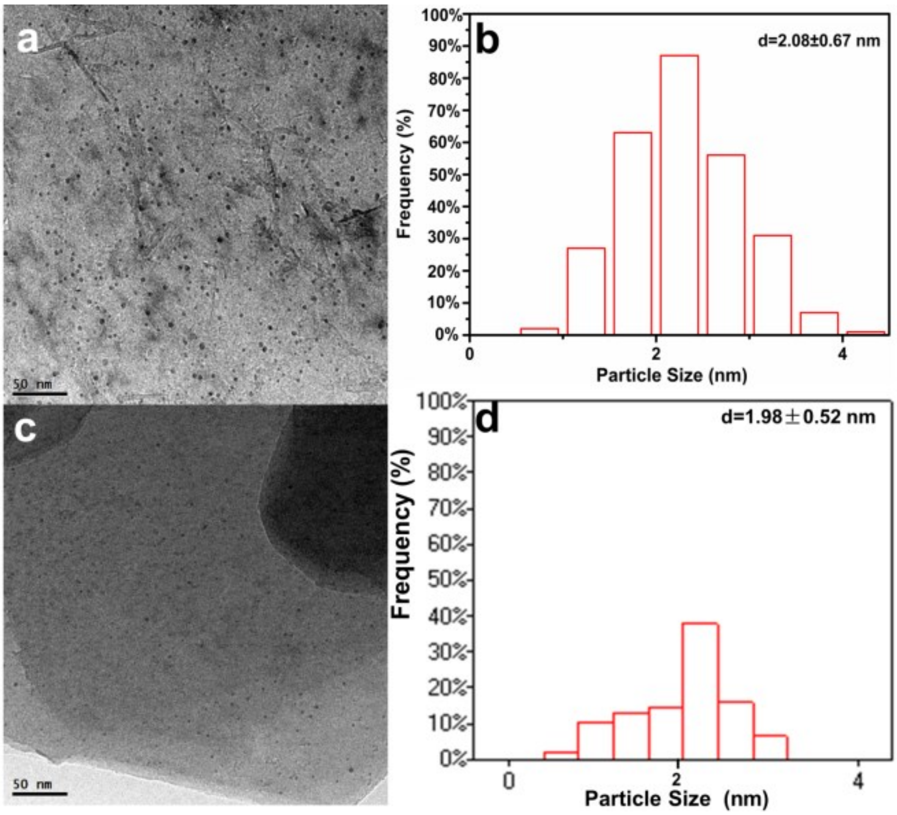

Fig. S10. Pd/MgAl-LDH: (a) TEM image. (b) Size distribution of the Pd cluster; Pd/ZnMgAl-LDH: (c) TEM image. (d) Size distribution of the Pd cluster.

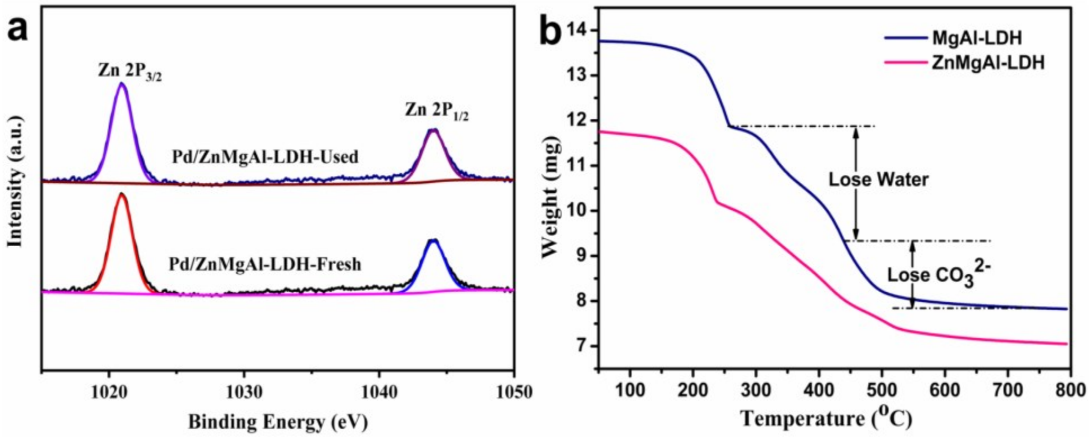

Fig. S11. (a) High-resolution XPS spectra of fresh and used Pd/ZnMgAl-LDH. (b) TG-DTA image of MgAl-LDH and ZnMgAl-LDH supports.

The TG-DTA spectra of the prepared samples are shown in Fig. S11b, the structure of LDHs remain not change when the temperature is below 200 °C, which is beneficial to thermal catalytic reaction.

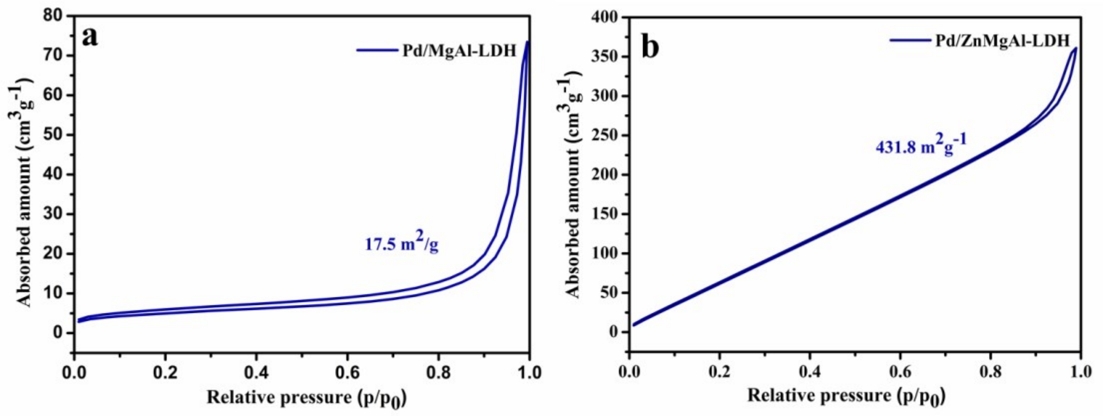

Fig. S12. N_2 adsorption-desorption isotherms. (a) Pd/MgAl-LDH. (**b**) Pd/ZnMgAl-LDH.

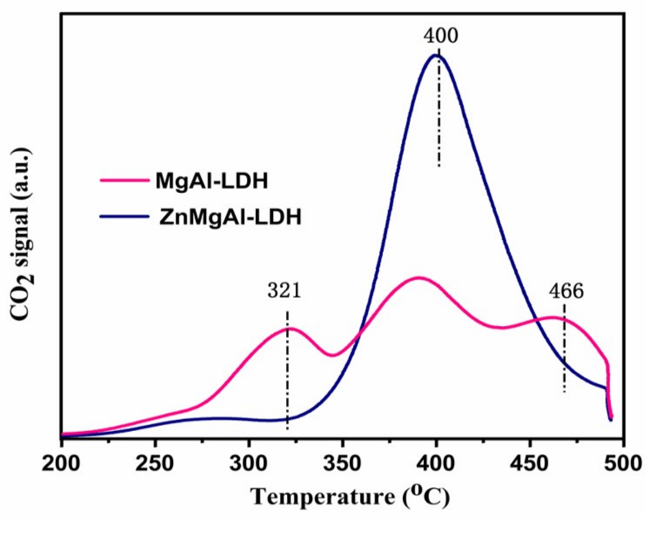

Fig. S13. CO_2-TPD profiles of the MgAl-LDH and ZnMgAl-LDH catalysts.

The CO_2-TPD spectra curves of ZnMgAl-LDH supports can be divided into three main desorption peaks, located at around 321 °C, 390 °C and 466 °C, respectively, which can be ascribed to the weak basic sites (OH groups), the moderate basic sites (M-O pairs, M represents metal cations) and strong basic sites (O^{2-} anions) [2].

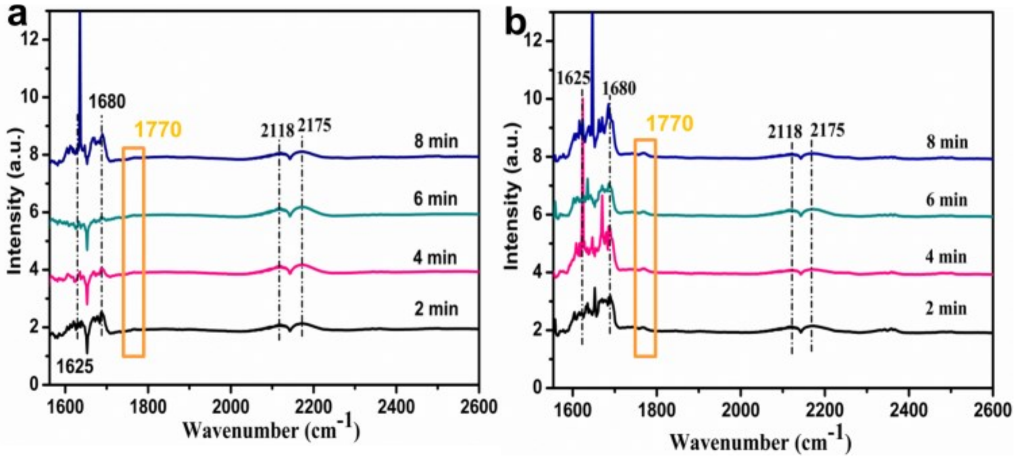

Fig. S14. In situ DR-FTIRS study of the CO adsorption the reaction of CO and methyl nitrite to DMO (a) Pd/MgAl-LDH. (**b**) Pd/ZnMgAl-LDH.

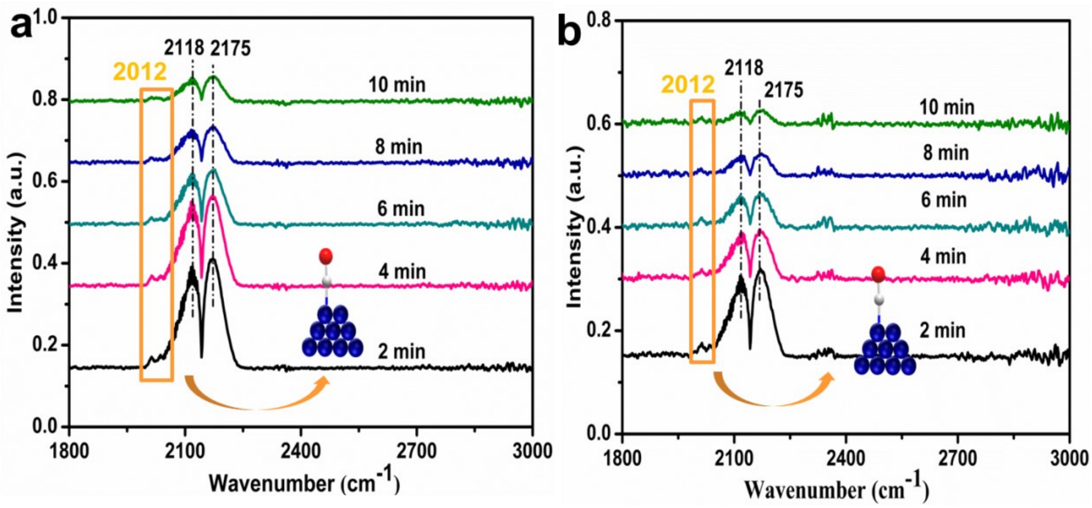

Fig. S15. *In situ* DR-FTIRS study of the CO adsorption (a) Pd/MgAl-LDH. (**b**) Pd/ZnMgAl-LDH.

In situ DR-FTIRS studies of the CO adsorption were employed to further illustrate the surface chemical property of a noble metal on supported catalysts. As shown in Fig. S15a and b, the *in situ* DR-FTIRS spectra of CO show that the absorption band of CO located at 2012 cm^{-1} appears both Pd/ZnMgAl-LDH and Pd/MgAl-LDH catalysts, indicating that the linearly adsorbed CO is connected with Pd clusters. The bands at 2118 and 2175 cm^{-1} are ascribed to CO in the gaseous state[3,4].

Supporting Tables

Table S1. CO oxidative coupling to DMO over different catalysts[a]

Entry	Catalysts	Actual Pd loading (%)	Conversion of CO (%)	Selectivity to DMO (%)	STY of DMO[b] ($g\cdot L^{-1}\cdot h^{-1}$)
1	Pd/MgAl-LDH(1:1)-Imp	0.75	42.9	93.9	892
2	Pd/MgAl-LDH(3:1)-Imp	0.79	48.6	91.7	986
3	Pd/MgAl-LDH(2:1)-Imp	0.78	52.75	92.8	1084
4	Pd/ZnMgAl-LDH-Imp	0.686	58.25	99	1277
5	Pd/ZnO[5]	0.5	67	98	1454
6	Pd/Mg–ZnO[5]	0.5	68	98	1476
7	Pd/MgO[6]	0.5	63	97	1353
8	Pd/α–Al_2O_3[6]	0.5	56	94	1166
9	Pd/MgAl-LDO-Imp	0.39	10.83	85.3	204
10	Pd/ZnMgAl-LDO-Imp	0.45	12.63	86.4	242

[a] Reaction conditions: 200 mg of catalyst, 3000 h^{-1} of gas hourly space velocity (GHSV), reactants CO/CH_3ONO volume ratio 1.56, 0.1 MPa, 130 °C.

[b] STY represents the space-time yield, grams of DMO per liter of catalyst per hour ($g\cdot L^{-1}\cdot h^{-1}$).

TOF values were calculated as the following equation:

$$TOF = (Fgas \times C_{CO} \times X_{CO}/1000/22.4)/(m_{cat} \times m_{Pd} \times D/M_{Pd}\times 60)(s^{-1})$$ [7]

Where F gas is the total flow rate, C_{CO} is the concentration of CO in gas mixture, X_{CO} is the conversion of CO, m_{cat} is the mass of catalyst (g), m_{Pd} is the mass of Pd in catalysts, D is the Pd dispersion obtained from CO chemisorption, M_{Pd} is the Pd molar weight.

Table S2. The dispersion and surface area of Pd for Pd/MgAl-LDH and Pd/ZnMgAl-LDH catalysts obtained from CO pulse chemisorption.

Catalysts	Pd dispersion (%)	Pd surface area (m^2/g-catalyst)

Pd/MgAl-LDH	47.38	0.16
Pd/ZnMgAl-LDH	26.72	0.12

Table S3. Fitting parameters of Zn K-edge EXAFS spectra for Pd/ZnMgAl-LDH.

Sample	Zn-O		Zn-Pd		D. W.	ΔE_0 (eV)
	R (Å)	CN	R (Å)	CN		
Pd/ZnMgAl-LDH	2.03±0.02	3.7±0.6	2.95±0.05	1.2±1.2	0.003(O) 0.006(Pd)	4.3±4.7

R: bonding distance; CN: coordination number; D. W.: Debey-Waller factor; E_0: inner potential shift.

Table S4. The calculated adsorption energies value.

$E_{sp}+E_{pd13}$ (eV)		$E_{pd13/sp}$ (eV)	E_{abs} (eV)
MgAl-LDH	Pd_{13}	Pd_{13}/MgAl-LDH	
-1306.32	-47.95	-1363.25	8.97
ZnMgAl-LDH		Pd_{13}/ZnMgAl-LDH	
-1303.18		-1362.75	11.61

References

1. S. Kumar, M. A. Isaacs, R. Trofimovaite, L. Durndell, C. M. A. Parlett, R. E. Douthwaite, B. Coulson, M. C. R. Cockett, K. Wilson, A. F. Lee, *Appl. Catal. B: Environ*, 2017, **209**, 394-404.
2. D. P. Debecker, E. M. Gaigneaux, G. Busca, *Chem. Eur. J*, 2009, **15**, 3920-3935.
3. B. T. Qiao, A. Q. Wang, X. F. Yang, L. F. Allard, Z. Jiang, Y. T. Cui, J. Y. Liu, J. Li, T. Zhang, *Nat. Chem*, 2011, **3**, 634-641.
4. T. Baidya, P. Bera, B. D. Mukri, S. K. Parida, O. Kröcher, M. Elsener, M. S. Hegde, *J. Catal*, 2013, **303**, 117-129.
5. S.-Y. Peng, Z.-N. Xu, Q.-S. Chen, Z.-Q.Wang, D.-M. Lv, J. Sun, Y.-M. Chen, G.-C. Guo, *ACS Catal*, 2015, **5**, 4410-4417.
6. S.-Y. Peng, Z.-N. Xu, Q.-S. Chen, Z.-Q.Wang, Y.-M. Chen, D.-M. Lv, G. Lu, G.-C. Guo, *Catal. Sci. Technol*, 2014, **4**, 1925-1930.
7. M. Boudart, *Chem. Rev*, 1995, **95**, 661-666.